(12)

DNA-TR-81-106

A COMPARATIVE ANALYSIS OF EQUATORIAL SPREAD F AND VHF SCINTILLATION

Roland T. Tsunoda Charles L. Rino
SRI International
333 Ravenswood Avenue
Menlo Park, California 94025

1 February 1982

Technical Report

CONTRACT No. DNA 001-81-C-0188

APPROVED FOR PUBLIC RELEASE;
DISTRIBUTION UNLIMITED.

THIS WORK WAS SPONSORED BY THE DEFENSE NUCLEAR AGENCY
UNDER RDT&E RMSS CODE X322081469 Q93QAXHX00001 H2590D.

Prepared for
Director
DEFENSE NUCLEAR AGENCY
Washington, DC 20305

Destroy this report when it is no longer needed. Do not return to sender.

PLEASE NOTIFY THE DEFENSE NUCLEAR AGENCY, ATTN: STTI, WASHINGTON, D.C. 20305, IF YOUR ADDRESS IS INCORRECT, IF YOU WISH TO BE DELETED FROM THE DISTRIBUTION LIST, OR IF THE ADDRESSEE IS NO LONGER EMPLOYED BY YOUR ORGANIZATION.

UNCLASSIFIED

SECURITY CLASSIFICATION OF THIS PAGE (When Data Entered)

REPORT DOCUMENTATION PAGE		READ INSTRUCTIONS BEFORE COMPLETING FORM
1. REPORT NUMBER DNA-TR-81-106	2. GOVT ACCESSION NO. AD-A133 219	3. RECIPIENT'S CATALOG NUMBER
4. TITLE (and Subtitle) A COMPARATIVE ANALYSIS OF EQUATORIAL SPREAD F AND VHF SCINTILLATION		5. TYPE OF REPORT & PERIOD COVERED Technical Report 6. PERFORMING ORG. REPORT NUMBER SRI Project 3388
7. AUTHOR(s) Roland T. Tsunoda Charles L. Rino		8. CONTRACT OR GRANT NUMBER(s) DNA 001-81-C-0188
9. PERFORMING ORGANIZATION NAME AND ADDRESS SRI International 333 Ravenswood Avenue Menlo Park, CA 94025		10. PROGRAM ELEMENT, PROJECT, TASK AREA & WORK UNIT NUMBERS Task Q93QAXHX-00001
11. CONTROLLING OFFICE NAME AND ADDRESS Director Defense Nuclear Agency Washington, D.C. 20305		12. REPORT DATE 1 February 1982 13. NUMBER OF PAGES 46
14. MONITORING AGENCY NAME & ADDRESS(if different from Controlling Office)		15. SECURITY CLASS (of this report) UNCLASSIFIED 15a. DECLASSIFICATION/DOWNGRADING SCHEDULE N/A since UNCLASSIFIED

16. DISTRIBUTION STATEMENT (of this Report)

Approved for public release; distribution unlimited.

17. DISTRIBUTION STATEMENT (of the abstract entered in Block 20, if different from Report)

18. SUPPLEMENTARY NOTES

This work was sponsored by the Defense Nuclear Agency under RDT&E RMSS Code X322081469 Q93QAXHX00001 H2590D.

19. KEY WORDS (Continue on reverse side if necessary and identify by block number)

Equatorial Spread F
Striations
Scintillation
Ionosonde

20 ABSTRACT (Continue on reverse side if necessary and identify by block number)

This report describes a series of simultaneous high-resolution ionosonde and VHF scintillation measurements made at Kwajalein during August 1981, a period of intense equatorial spread-F. The scintillation data were processed to measure the Doppler spread, which was found to be closely correlated with a recurrent ionogram pattern of oblique echoes, h'F variations, and range spread. The ionogram patterns are evidently due

DD FORM 1 JAN 73 1473 EDITION OF 1 NOV 65 IS OBSOLETE

UNCLASSIFIED

SECURITY CLASSIFICATION OF THIS PAGE (When Data Entered)

20. ABSTRACT (Concluded)

to the overhead passage of bottomside F-region upwellings. The combined measurements provide a comparatively simple means of monitoring spread-F activity.

The report also reviews five years of summertime ionosonde measurements made at Kwajalein that show dramatic ionospheric changes with increasing solar cycle activity. The results are discussed in light of global occurrence patterns and the behavior of polarization fields at the equator.

EXECUTIVE SUMMARY

Over the past 5 years the Defense Nuclear Agency (DNA) has supported regular observations of equatorial spread-F activity at Kwajalein during the local summer months when there is a high probability of enhanced activity. The broad objective of this research was to measure the onset, evolution, and decay of the intense intermediate-scale irregularities associated with equatorial spread-F. The basic convective instability that causes this structure to develop is operative at late times after high-altitude nuclear detonations and can produce long-lasting disruptions of satellite communication, navigation, and surveillance systems.

Until 1981, the ALTAIR/TRADEX radars played a prominent role in these equatorial research campaigns. In 1979 the ALTAIR radar was used to target high-performance rockets instrumented to measure spread-F irregularities in situ as a part of an elaborate experiment called PLUMEX. HF sounder and scintillation measurements were routinely made during these campaigns. This research has been very successful in providing a detailed definition of the intermediate-scale structure, and the level-of-effort and scope of the work have been changed accordingly. Thus, the current measurement campaign was designed to measure the onset and decay phase of equatorial spread-F, because a number of important questions remain unanswered.

Unfortunately, heavy demands on the ALTAIR radar precluded its use during the summer of 1981. However, we were able to obtain two weeks of simultaneous, high-time-resolution HF sounder data and VHF scintillation data from the geosynchronous FLTSATCOM satellite. This report summarizes the results from the 1981 measurements. Preparing it also provided an opportunity to review the entire data base of HF sounder measurements made at Kwajalein since 1977, the collective results of which provide some important clues on the necessary conditions for equatorial spread-F occurrence.

An important result from the 1981 observations, however, is that the combined observations from an HF sounder and a continuous scintillation monitor can be used to detect and localize spread-F structures. Thus, these comparatively simple and inexpensive monitors can be used for future field campaigns that need such information, but may not have access to or resources to support sophisticated backscatter radar measurements.

A number of unanswered questions remain regarding the onset and occurrence patterns of equatorial spread-F. Nonetheless, naturally occurring equatorial spread-F is a ready source of intense, well-diagnosed structure that can be used to evaluate the performance of various systems in disturbed propagation environments. As an example, as yet there is no verified theory that can be used to reliably predict the enhanced delay and Doppler spread on HF modes that pass through striated regions. Indeed, such effects are not incorporated in existing nuclear effects codes. The diagnostic methods developed under this contract and summarized in this report can be used to locate the structured regions if equatorial HF experiments are conducted to obtain data on this phenomenon.

PREFACE

The assistance of N. B. Walker in analyzing the scintillation data and M. D. Cousins for assistance with the field operations is gratefully acknowledged.

TABLE OF CONTENTS

LIST OF ILLUSTRATIONS

I INTRODUCTION

The ionospheric irregularities that develop in the nighttime equatorial F layer, which are collectively referred to as equatorial spread F (ESF), are characterized by a spectral density function that subtends six orders of magnitude in wavelength (< 10 cm to > 100 km). Considerable progress has been made over the last decade in understanding the dynamic evolution of large-scale equatorial plasma-density depletions or bubbles,[1*] which manifest themselves in a variety of ways, e.g., radar backscatter plumes[2] and dark bands in 6300-Å airglow all-sky maps.[3,4] Numerical simulations of the equatorial ionosphere have reproduced all the main features of the plumes.[5-7] Indeed, the most recent analyses by Zalesak et al.[5] have accommodated the velocity-sheer effects[8,9] produced by an eastward neutral wind and a finitely conducting E layer at the ends of the unstable geomagnetic flux tubes.

Radar backscatter and incoherent scatter measurements using the fully steerable ALTAIR and TRADEX radars, located near the geomagnetic equator in the Pacific sector, have added considerably to our detailed knowledge of the onset, dynamic evolution and decay of backscatter plumes.[9-12] Indeed, understanding the physics of the small-scale irregularities that cause the enhanced backscatter is progressing rapidly.[11,13-16]

On the other hand, the intermediate-scale structures (one to several tens of kilometers) that dominate the scintillation characteristic at UHF and VHF are only beginning to be understood. The PLUMEX rocket campaign conducted at Kwajalein in 1979 provided the first definitive measurements of the entire irregularity continuum.[17-20] In these experiments, it was shown, for example, that in the regions where the most intense intermediate-scale structure develops, the spectral

---

*The references are listed at the end of this report.

density function has a two-component power-law form with the transition occurring above the spatial wavenumber corresponding to one kilometer.

The PLUMEX rocket carried a downward-looking multifrequency beacon which provided a unique opportunity to relate scintillation structures unambiguously with the characteristics of the irregularities that cause the scintillation. A comparative analysis by Rino et al.[19] of the beacon data, in situ electron density probe data, and radar backscatter maps made by the ALTAIR radar have shown that the most intense intermediate-scale irregularities develop in high-density regions adjacent to the depletions. Moreover, the analysis confirms the systematic decrease of the spectral index with increasing perturbation strength reported by Livingston et al.[21]

To study the intermediate-scale irregularities associated with ESF further and their interrelationship with the large-scale ionospheric plasma configuration, a series of comparatively simple diagnostic measurements were made using an ionosonde and a VHF scintillation monitor at Kwajalein during August 1981.

The sounder produced a film-recorded ionogram every 20 seconds so that the dynamics of the equatorial ionosphere, as indicated by h'F (the minimum virtual height of the F layer) and the occurrence of oblique echoes, could be continuously monitored along with the occurrence of classical spread F. Under conditions of strong ESF, VHF intensity scintillation is generally saturated. Nonetheless, the coherence time of the intensity scintillation, which is inversely proportional to the Doppler spread, varied systematically during sustained periods of enhanced ESF.

We found that the largest Doppler-spread enhancements were invariably accompanied by a pattern of oblique echoes and local upwelling of the F-layer that we have identified with the overhead transversals of large depletions. The result was expected in light of the association of broad scintillation patches with radar backscatter plumes,[22] although the Doppler signature in VHF intensity scintillation had not been demonstrated previously.

We have also reviewed a large body of HF sounder data recorded at Kwajalein during other local summer periods when there was a high occurrence of ESF. The layer height variation followed the same pattern as reported by Fejer[23] who analyzed data from the Jicarmarca radar. These results are discussed in light of the yet unexplained global/longitudinal/seasonal variations of ESF activity.

II EXPERIMENT

A. Ionosonde

To monitor the ionospheric state, an Australian made (KEL) ionosonde was operated on Roi-Namur Island, located at the northern tip of the Kwajalein Atoll (9.4013°N latitude, 167.4826°E longitude, ∿9° magnetic dip). The sounder is a swept-frequency, pulsed system designed for routine vertical-incidence sounding of the ionosphere. It employs a digital synthesizer that provides frequency coverage from 1 MHz to 22.6 MHz in 576 logarithmic steps. The frequency sweep takes 12 s of a 20-s program cycle that produces a conventional ionogram record.

The ionosonde features selectable programming from one sounding every 15 min to three soundings per minute--the "continuous mode" of operation. For the August 1981 experiment, the continuous mode was used exclusively to record automatically on 100-ft reels of 16-mm film. The 100-ft reels lasted about 22 hours and were changed daily around local noon.

Crossed-delta antennas, 65 ft high at the vertex and 130 ft across the base of the triangle, were used, one for transmission and one for reception. Both antennas were oriented ±45° with respect to Magnetic North to preserve both the O and X modes.

B. Scintillation Receiver

To monitor the VHF propagation disturbances associated with the severe nighttime spread-F that is routinely observed at Kwajalein during the summer months,[24] a 244-MHz continuous-wave (CW) signal was recorded. The signal was transmitted by the FLTSATCOM satellite, which is in geosynchronous orbit at 172°E longitude. The line-of-sight to the satellite subtended a 77.37° elevation angle at 154.42° true azimuth.

With this viewing geometry, the ionospheric penetration point at a height of 400 km was located 86 km southeast of Roi Namur. The geomagnetic east-west separation of the ionospheric penetration point from the magnetic field line through Roi Namur was 47 km. Thus, for a typical eastward drift of 100 m/s, a field-aligned disturbance detected with the sounder would cross the line-of-sight to the scintillation monitor ∿8 min later.

The receiver system was a four-channel, VHF/UHF phase-coherent system designed and built by SRI International for the Air Force Geophysics Laboratory (AFGL). This "μ-Wideband receiver" can measure differential phase when two or more multifrequency phase-coherent signals are transmitted or it can measure a single signal against a stable local oscillator. The data are digitally recorded under control of a microcomputer system that automatically schedules the receiver operation.

For the Kwajalein experiments, data were recorded from two remote antennas--one on a 600-m east baseline and one on a 900-m south baseline--together with the data from the main channel. In this paper, however, we shall only discuss amplitude scintillation data collected on the main channel. Because of the severe propagation disturbances, the phase data are difficult to interpret. The spaced-receiver data can provide irregularity anisotropy and drift data;[23] however, these data have not yet been analyzed.

A summary of the data collected with the ionosonde and the μ-Wideband system is given in Table 1. The Julian day and date (universal time) are given in the first two columns, followed by the times of operation for each instrument. The μ-Wideband system was set up first, and it started to operate on August 13. The ionosonde was checked out and turned on a day later. Data were collected over 14 days; simultaneous measurements were obtained on all but three days.

Table 1

DATA SUMMARY

Day (UT)	Date (UT)	μWB (UT)	Ionosonde (UT)
225	13 August	1449 to 2121	No data
226	14 August	0700 to 1401	0502 to 2048
227	15 August	No data	0045 to 1446
228	16 August	1201 to 1859	0022 to 2300
229	17 August	0710 to 1900	0025 to 2130
230	18 August	0700 to 1900	0030 to 2255
231	19 August	0700 to 1900	0032 to 2233 2332 to 2400
232	20 August	0700 to 1043	0000 to 2012 2335 to 2400
233	21 August	0700 to 1352	0000 to 2104
234	22 August	0700 to 1310	0544 to 2056
235	23 August	0715 to 1900	0507 to 2400
236	24 August	0700 to 1900	0000 to 0204 0313 to 2400
237	25 August	0805 to 1900	0039 to 2331
238	26 August	0700 to 1900	0034 to 2305
239	27 August	No data	0000 to 2129

III RESULTS

A. Ionosonde Measurements

Ionograms, besides providing information on the general state of the ionosphere, can be used

(1) To determine the altitude of the nighttime equatorial F layer, and

(2) To detect the passage of highly structured regions in the F layer, those associated with plasma bubbles,[1] radar backscatter plumes,[2] and strong scintillations.[22,26]

Altitude variations of the nighttime F layer are important in understanding equatorial electrodynamics and the processes that produce ESF irregularities. The altitude of the bottomside of the F layer is assumed to be identical to the minimum virtual height of the F-layer trace, h'F. Bittencourt and Abdu[27] and Tsunoda and White[12] have shown that h'F is a reasonably accurate measure of the bottomside F-layer altitude when the altitude in question is above 300 km.

Passage of highly structured regions in the F layer over the ionosonde is manifested in three ways:

(1) By the occurrence and dynamics of oblique echoes,

(2) By large-scale variations in h'F with time, and

(3) By variations in range spread associated with the main F-layer trace.

The first two ionogram characteristics result from radiowave reflections from large-scale (few hundred kilometers) "upwellings" in the bottomside F layer. Upwellings are local depletions in F-region plasma density that can best be visualized as altitude modulations of isodensity contours in the bottomside F layer.[28] These upwellings also cause prominent dark bands in the 6300-Å airglow[3,4] and altitude variations in the bottomside field-aligned backscatter measured with VHF and UHF radars.[2,20,28]

1. General Characteristics: 1981 Data Set

Plots of h'F as a function of universal time (UT), for the 14 nights of operation in 1981, are presented in Figure 1. Local solar time (LST) leads UT by 11 hours 10 minutes. Julian Day 226 corresponds to August 14 and Day 239 to August 27. Solid circles are used in the plots to indicate h'F estimates made from ionograms taken during non-spread-F conditions, while asterisks indicate h'F estimates made from ionograms taken during spread-F conditions.

The typical behavior is a rapid increase in h'F beginning around E-region sunset (around 0700 UT), with h'F reaching a maximum altitude around 1950 LST (0840 UT), followed by a descent that is nearly as rapid. The rate of increase in h'F during the postsunset rise of the F layer ranged from 25 m/s to 55 m/s, with a mean rise velocity of 35 m/s. The maximum altitude reached by h'F as a result of the post-sunset rise ranged from 380 km to 490 km, with a mean altitude of 426 km. The reversal time from an increasing h'F to a decreasing h'F ranged from 1855 LST to 2000 LST, with a mean reversal time of 1931 LST.

Besides the increase in h'F associated with the postsunset rise of the F layer, there is often a quasi-oscillatory variation in h'F. The most pronounced example is in the Day 229 curve, although oscillatory behavior is evident on most disturbed nights. Whether the absence of oscillatory variations in h'F on quiet nights is a general characteristic is not known. The h'F curve for Day 233, the only quiet night in the data set, is relatively free of oscillatory variations in h'F. These quasi-periodic variations in h'F are believed to be associated with the passages of upwellings in the bottomside F layer. The relationship of these h'F variations to radio-wave scintillations and to the occurrence of oblique echoes in ionograms is determined in Sections III.B and III.C.

Spread-F activity in the curves in Figure 1 begins around the time that h'F reaches its maximum altitude. Sometimes ESF activity begins during conditions of increasing h'F, and sometimes during conditions of decreasing h'F. Thus, the occurrence of ESF activity appears

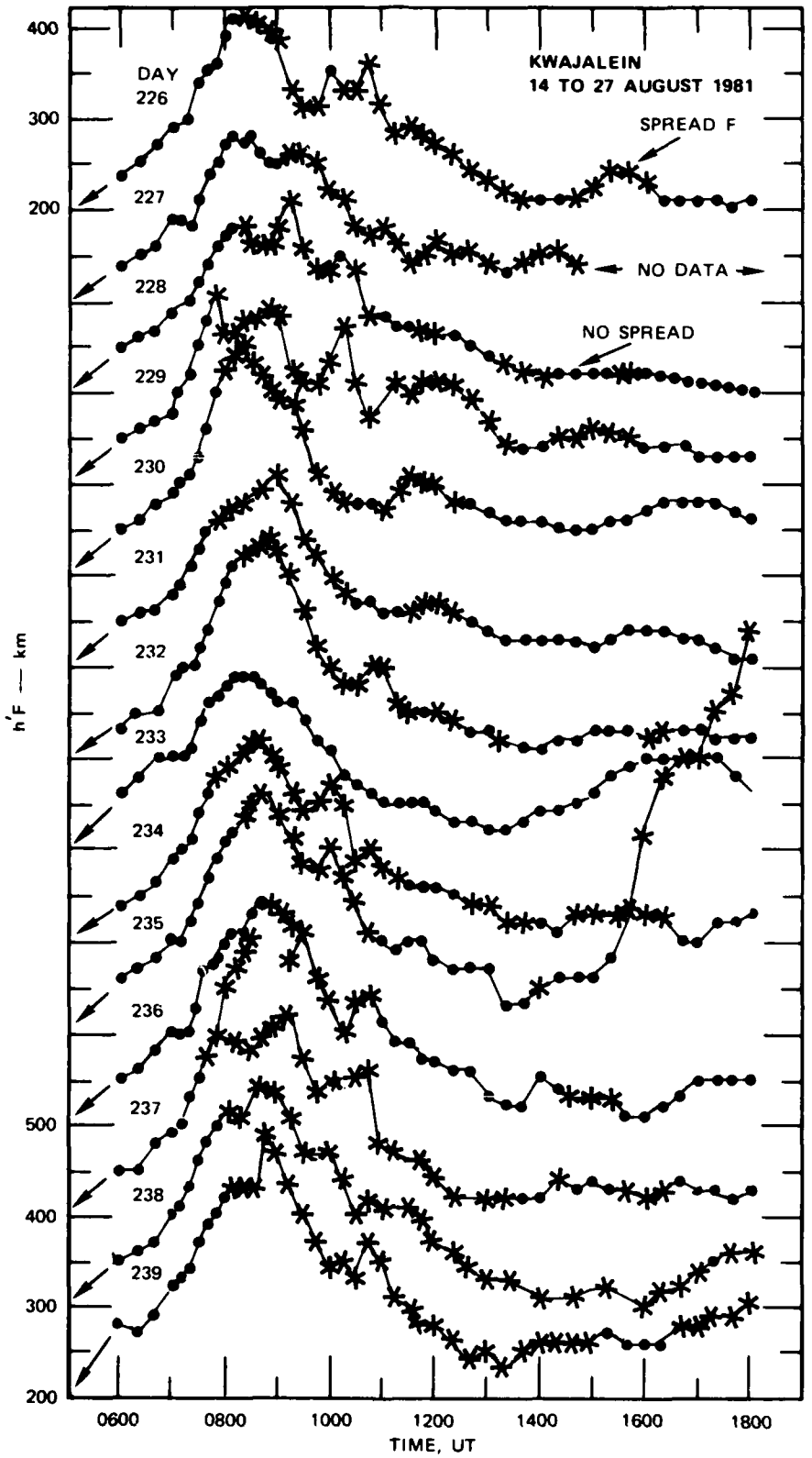

FIGURE 1 DIURNAL VARIATION OF h'F MEASURED AT KWAJALEIN ON 14 TO 27 AUGUST 1981

to favor large values of h'F, a characteristic of ESF activity pointed out earlier by Farley et al.[29] A spectacular example ESF activity occurs during the existence of large h'F values on Day 235, when h'F increased dramatically from 260 km at 1500 UT to 640 km by 1800 UT. Spread F developed by 1530 UT and persisted until the development of a sunlit F layer.

Achieving a critical F-layer height is not a sufficient condition for the development of ESF, although it seems to be a necessary one. To demonstrate this, we have plotted the h'F curves from Days 227 and 233 together in Figure 2. From Figure 1, we note that ESF occurred on Day 227, but not on Day 233. Despite the absence of ESF activity on Day 233, we find that the h'F curves are very similar. During the period of ESF activity, the average difference in h'F from the two days was no more than about 20 km. This kind of evidence has been used to argue for the need of a controlling mechanism other than reduced collisional damping.

2. Solar Activity Dependence

Comparisons of h'F characteristics found in Figure 1 can be made with h'F characteristics observed during earlier years. Plots for the years 1977 and 1979 are presented in Figures 3 and 4. The 1977 h'F values were obtained from Bibl et al.[30] The 1979 data were collected by SRI International in support of the PLUMEX rocket campaign.[17-20] The major difference between the h'F curves in Figures 3 and 4 and those in Figure 1 is the less-developed nature of the postsunset rise of the F layer. The mean value of the highest h'F for 1981 is 426 km. In comparison, the mean values of the highest h'F for 1977 and 1979 are 299 km and 373 km, respectively. These altitudes are lower by 127 km and 53 km from those for 1981. These lower peak altitudes, as might be expected, are associated with smaller F-layer vertical velocities. The mean rise velocity for 1981 was 35 m/s, compared to 9 and 23 m/s for 1977 and 1979. The descent velocities are nearly the same as the ascent velocities; thus, the period that the F layer remains above 300 km, for example, is similar for 1979 and 1981.

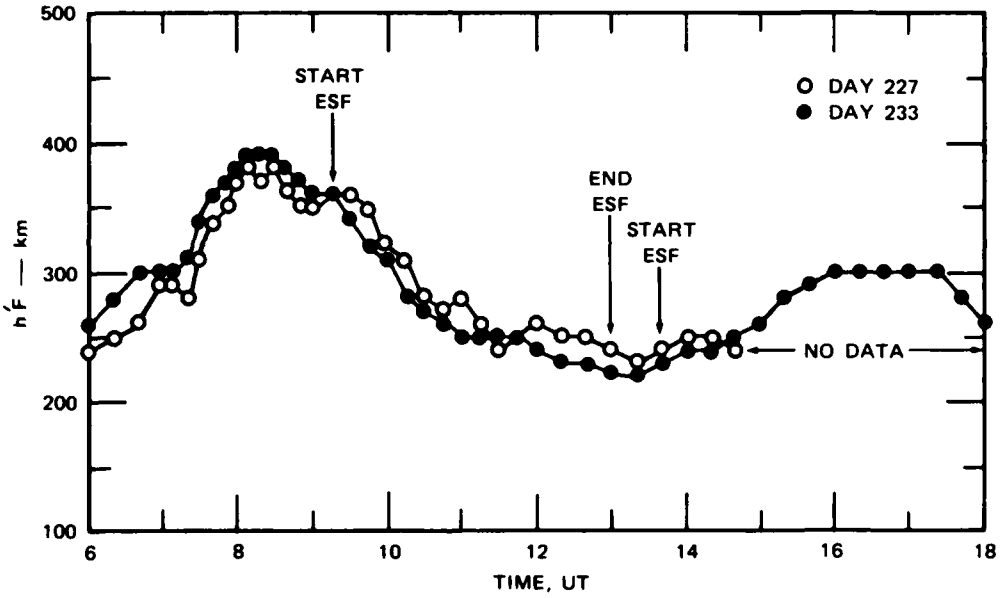

FIGURE 2 SUPERPOSITION OF 1981 KWAJALEIN h'F MEASUREMENTS FROM DAY 227 AND DAY 233

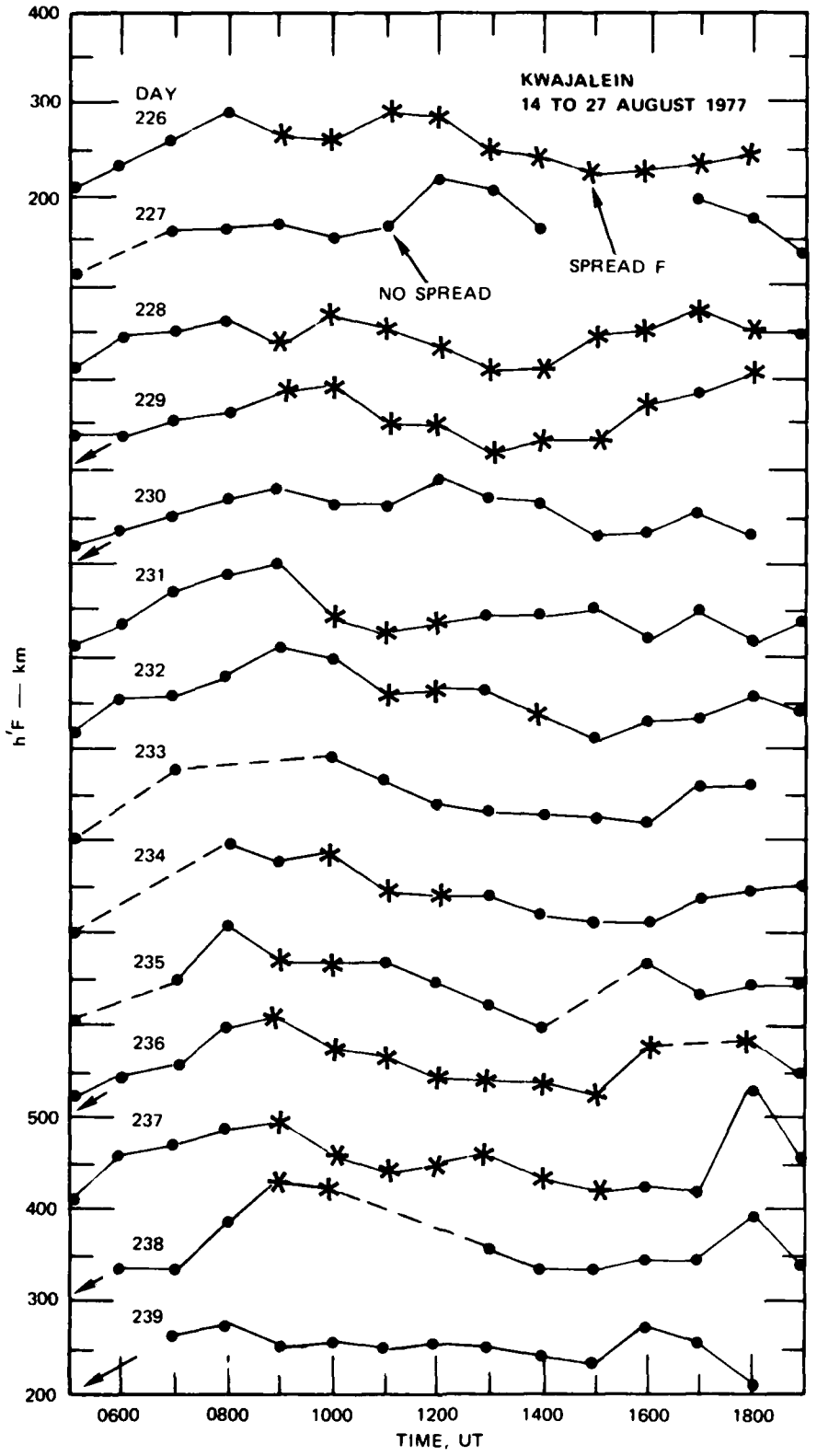

FIGURE 3 DIURNAL VARIATION OF h'F MEASURED AT KWAJALEIN DURING AUGUST 1977 UNDER SOLAR MINIMUM CONDITIONS

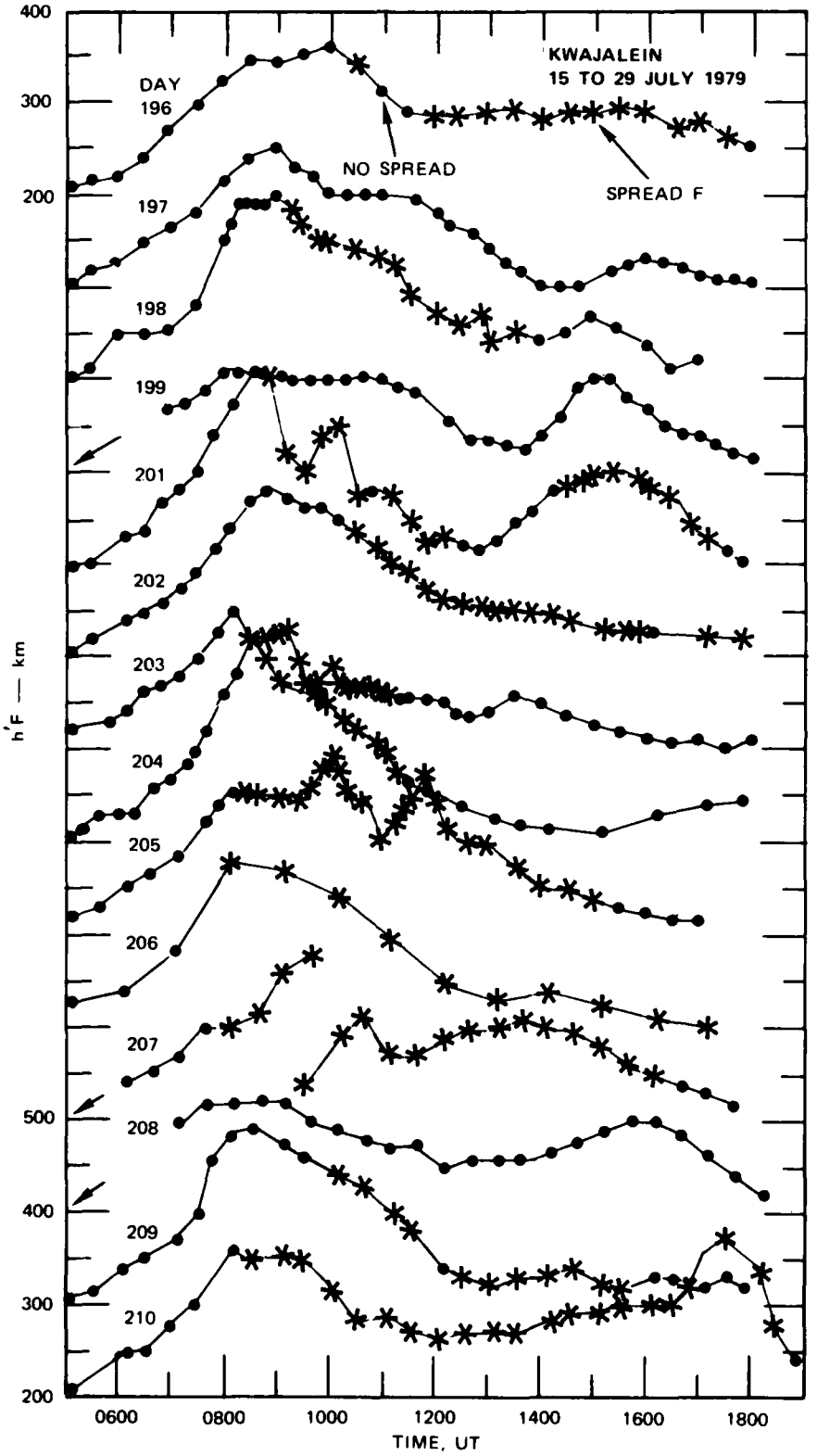

FIGURE 4 DIURNAL VARIATION OF h'F MEASURED AT KWAJALEIN DURING AUGUST 1979

Both the occurrence and severity of ESF is evidently associated with solar activity. The mean sunspot numbers for 1977, 1979, and 1981 were 33, 137, and 197, respectively. As can be seen from Figures 1, 3, and 4, ESF occurred on 13 of 14 nights during 1981 as compared to 11 of 14 nights in 1979 and 10 of 14 nights in 1977. Moreover, ESF activity in 1977 was often short-lived, lasting for no more than an hour or so on five of 10 active nights.

The large postsunset rise velocities and high values of h'F should be associated with the formation of the equatorial anomaly by the "fountain" effect.[31] That is, plasma lifted by E × B motion at the magnetic dip equator diffuses down along geomagnetic field lines to enhance the plasma density at higher latitudes. This effect can be seen in the total electron content (TEC) results obtained with the Wideband satellite as reported by Livingston in Rino et al.[19] The latitudinal distribution of TEC obtained from Wideband satellite measurements made at Kwajalein from 1976 through 1979 is shown in Figure 5. Examining the panels for the months July and August, we see that build-up in TEC at higher latitudes was negligible in 1977, significant in 1978, and largest in 1979. Although TEC data were not collected in 1981 from Kwajalein, the trend is clearly consistent with the behavior of the h'F curves in Figures 1, 3, and 4.

3. Longitudinal Dependence

The Kwajalein h'F characteristics can be compared to results obtained at other longitudes to shed some light on the question of longitudinal dependence of ESF and scintillation activity. Both in situ[32,33] and scintillation[34] measurements indicate that the six-month difference in the seasonal scintillation maximum between the Asian (e.g., Kwajalein) and American (e.g., Jicamarca, Peru) sectors is a true longitudinal difference, and not simply a local seasonal variation. Burke et al.[33] proposed that the Earth's eccentric dipole magnetic field could produce growth rates of irregularities that is faster in the American sector than in the Asian sector. This longitudinal difference, however, cannot account for the observed six-month phase difference in scintillation

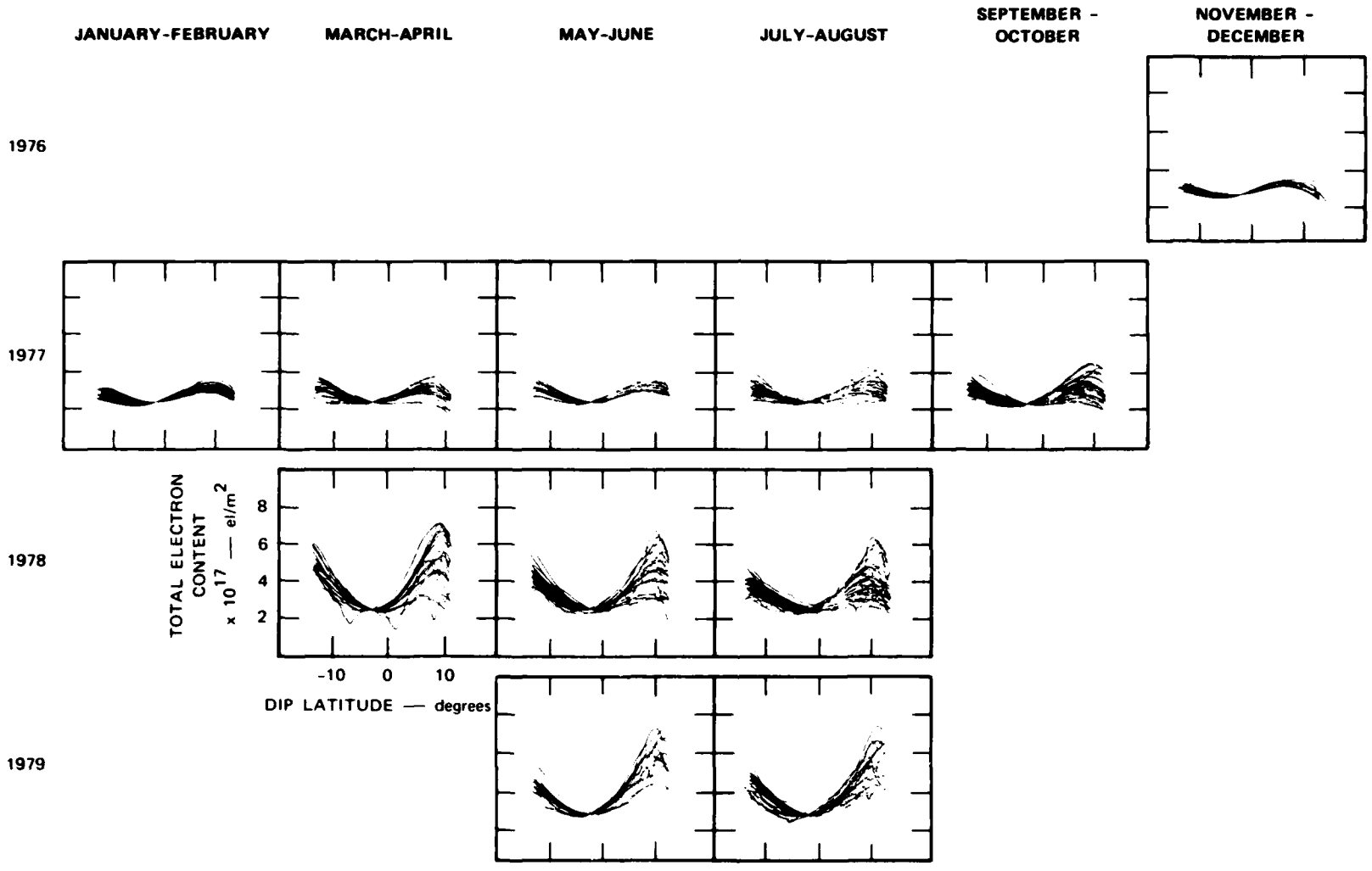

FIGURE 5 LATITUDINAL DISTRIBUTION OF TEC AT KWAJALEIN DERIVED FROM WIDEBAND SATELLITE DATA

maxima. Thus, in this subsection, we review results from other longitudes, in particular those obtained at Jicamarca, and compare them to the h'F characteristics obtained for Kwajalein.

Woodman[35] made incoherent-scatter Doppler measurements at Jicamarca from 1968 to 1970 (sunspot maximum) and found postsunset rise (prereversal enhancement) velocities as high as 50 m/s. From his velocity plots, we found that average velocities were close to 40 m/s, which agrees with the 35 m/s in the 1981 Kwajalein results. The nighttime downward velocity immediately after the reversal was also similar to the postsunset rise velocity, as we noted in the Kwajalein data.

Woodman et al.[36] analyzed the solar cycle dependence of the vertical velocity and found that the postsunset rise velocity is characteristic of solar maximum, but missing (except occasionally during equinoxes) during the solar minimum period. The solar cycle dependence is clearly evident in the Kwajalein results (Section II.B.2). Woodman et al.[36] also found that the absence of the prereversal enhancement in upward velocity (postsunset rise of the F layer) resulted in the shifting of the velocity reversal to earlier times. During solar maximum, the reversal time at Jicamarca occurred around 1920 LT (with individual times ranging from 1830 to 2030 LT). During solar minimum, the reversal time occurred around 1850 LT. Fejer et al.[37] also reported similar results using a more complete Jicamarca data set, although they found that the reversal time occurred two hours earlier during solar minimum than during solar maximum. The mean reversal time over Kwajalein in 1981 was 1931 LST, in excellent agreement with the mean reversal time over Jicamarca. (No attempt was made to estimate the reversal times in the Kwajalein data for 1977 and 1979.)

The fact that the electrodynamics of the F layer has a similar solar cycle dependence at both Jicamarca and Kwajalein is significant because the two stations have seasonal differences in ESF activity. Livingston[24] showed that scintillation activity at Kwajalein and Ancon, Peru (near Jicamarca) both have a broad eight- to nine-month maximum centered on local summer, but, because Ancon (and Jicamarca) are in the

Southern Hemisphere, the scintillation activity maximum occurs six months out of phase with that at Kwajalein. Aarons et al.[34] argued that this difference must depend on longitude because the scintillation activity at Accra, Ghana (Northern Hemisphere) is similar to that at Huancayo, Peru (Southern Hemisphere).

Fejer[23] compared the reversal time (from upward by day to downward by night) as a function of time of year at Huancayo and Kodaikanal. This comparison is of interest because Huancayo is located near Jicamarca and Kodaikanal (India) is reasonably close to Kwajalein. Fejer[23] found that the reversal time variations at Kodaikanal was similar to that at Jicamarca (during solar maximum) but shifted by six months. The latest reversal time at Kodaikanal occurred in mid-June. Fejer[23] attributed the six-month shift to the locations of the stations in opposite hemispheres. The local time of reversal in July-August at Kodaikanal is around 2000 LT, about 30 minutes later than observed at Kwajalein. As noted earlier, late reversal times correspond to large postsunset rise velocities and high values of h'F. The summer maximum in reversal times at Kodaikanal suggests that h'F also reaches a summer maximum at Kwajalein.

The variations in vertical-velocity reversal time with local season is possibly caused by a meridional neutral wind. The wind typically blows from the Summer to the Winter Hemisphere,[38] causing an upward movement of plasma along the geomagnetic field lines in the Summer Hemisphere and a downward movement in the Winter Hemisphere. The meridional neutral wind, however, is opposed by an eastward neutral wind in locations that have an eastward magnetic declination. Even so, for the declination of Kwajalein (9°), a zonal wind that is six times the meridional wind is required to offset the effect of the meridional wind. The meridional neutral wind, therefore, can account for the seasonal variations in the postsunset rise of the equatorial F layer.

Now, if the variation of ESF activity were purely longitudinal, the seasonal variation in the postsunset rise velocity should not be a factor in the occurrence of ESF. Moreover, a purely longitudinal dependence suggests that the conditions for plasma structuring can be

completely described in terms of magnetic flux-tube-integrated quantities.[39] Field-line integration would remove any seasonal dependence. To complicate the issue further, a conducting E layer at the ends of the flux tubes can strongly influence the growth rate of instabilities.[5] Thus, further experimental and theoretical work will be required to resolve the detailed mechanism of ESF control.

B. Scintillation Measurements

It has been known for several years that there is a close association between the occurrence of VHF/UHF scintillation and ESF as measured on ionograms, backscatter radar RTI displays, and airglow sky maps.[40] For the most part, however, only the intensity scintillation level has been used for comparative analyses. Because the VHF intensity scintillation level is typically saturated for extended periods during ESF activity, such observations only give information about the onset and decay of the activity.

Rino and Owen[41,42] have shown, however, that under saturated conditions the intensity coherence time gives a very accurate measure of the perturbation strength integrated along the propagation path. Thus, in analyzing the FLTSATCOM data, we have computed both the intensity scintillation index, S_4, and the time delay to a 50-percent decrease in the intensity autocorrelation function.

For display purposes, we have used the Doppler spread, which we define as the reciprocal of the time to a 50-percent intensity correlation. This was done to obtain a measure directly proportional to the perturbation strength. The interpretation of the Doppler spread is potentially ambiguous because the conversion of the spatial structure to the temporal structure that is actually measured depends on the velocity component transverse to the line of sight.

The irregularity drift rates are, however, slowly changing quantities as indicated by the observation of plumes on backscatter radars. Moreover, we shall show that the Doppler spread enhancements are well correlated with a recurrent pattern of oblique echoes and local upwellings of the F layer.

The scintillation results are presented in two subsections. In the first, we describe the general characteristics of the S_4 index and the Doppler spread as a function of time. In the second, we relate the Doppler spread to oblique echoes seen in ionograms.

1. General Characteristics: S_4 Index and Doppler Spread

Plots of the computed S_4 index and Doppler spread for each of the 12 nights of operation listed in Table 1 are presented in Figure 6. The upper panels show the Doppler spread variation as a function of UT. The corresponding variation of S_4 is shown in the lower panels. Periods of ESF activity as scaled from the ionograms are indicated by the horizontal bars labeled ESF.

Figure 6(c) (Day 244) clearly reveals the general characteristics. There is an abrupt onset of scintillation at 0830 UT followed by nearly four hours of saturated intensity scintillation. The Doppler data show considerable variation during this period. Indeed, the characteristics of the Doppler spread enhancements are very similar in structure to scintillation patches observed at L band and the backscatter plumes, which are prominent features in radar backscatter RTI displays.

The S_4 index appears to saturate at a value near 0.75, not 1.0. This behavior has also been observed in UHF scintillation data measured by the Wideband satellite.[43,44] The observation can be explained as follows:

(1) Under strong scatter conditions, the scintillation structure at UHF (and lower frequencies) is dominated by irregularities with scale sizes greater than one kilometer--the intermediate-scale regime defined by Livingston et al.[21]

(2) In the intermediate-scale size regime, the power-law index is generally less than two and systematically decreases with increasing perturbation strength.[19,21]

(3) For such shallowly sloped spectra, the convergence of S_4 to unity with increasing perturbation strength occurs from below and is comparatively slow.[45] Thus, rather than a true saturation, the S_4 behavior is a consequence of increasing perturbation strength and systematically changing spectral characteristics.

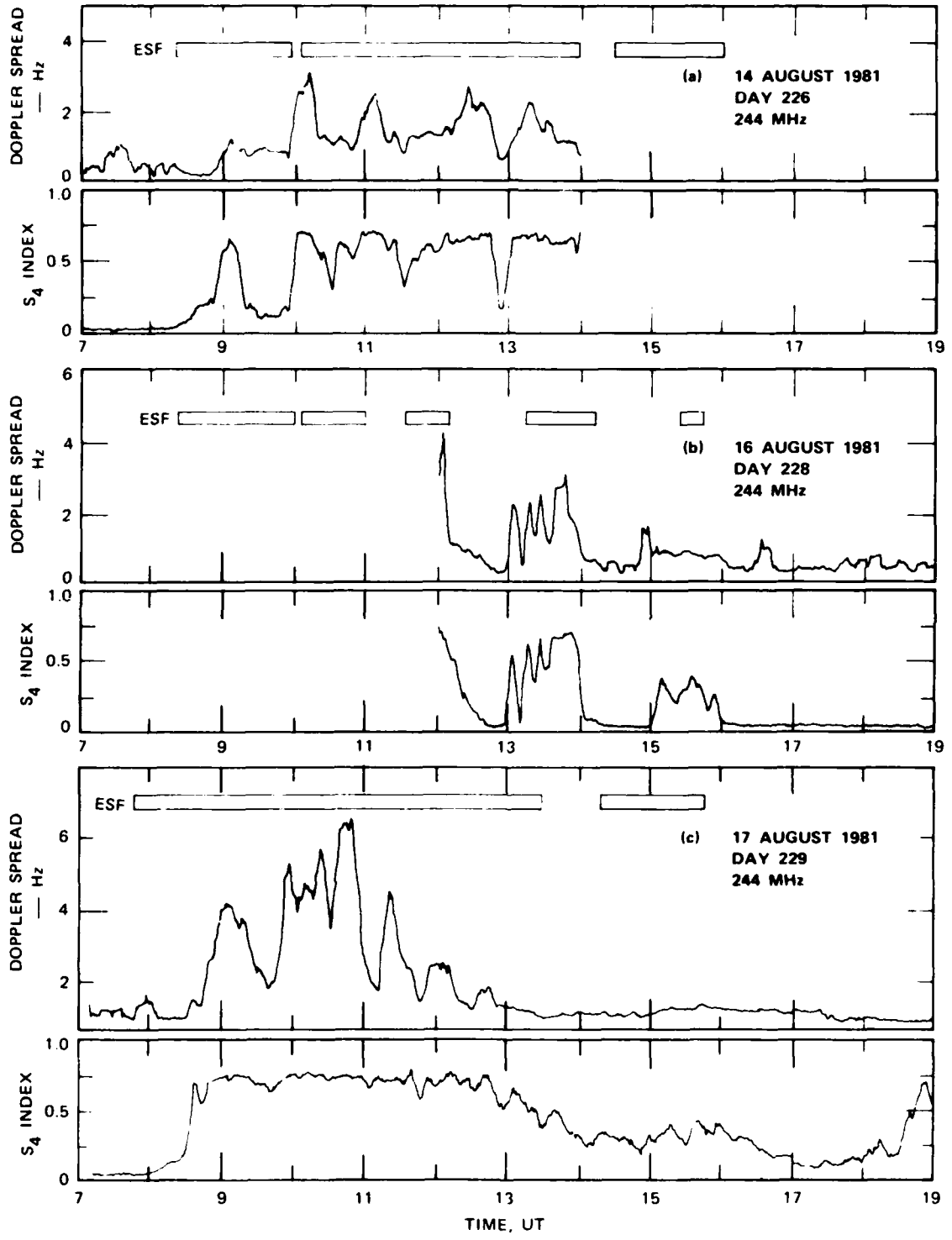

FIGURE 6 NIGHTTIME OCCURRENCE OF VHF INTENSITY SCINTILLATION AND ENHANCED DOPPLER SPREADING AT KWAJALEIN DURING AUGUST 1981. The horizontal bars indicated periods of ionogram spread F.

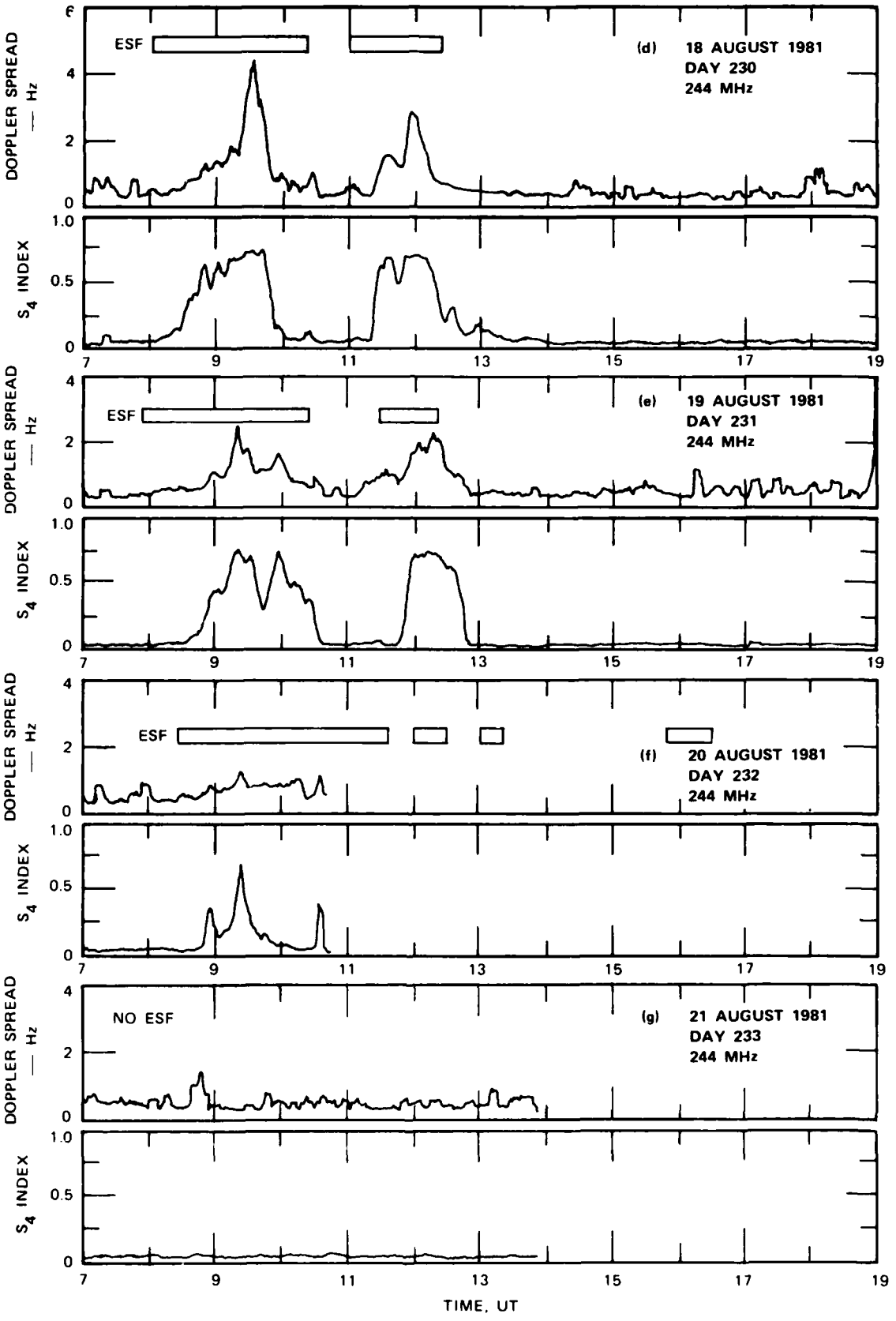

FIGURE 6 (Continued)

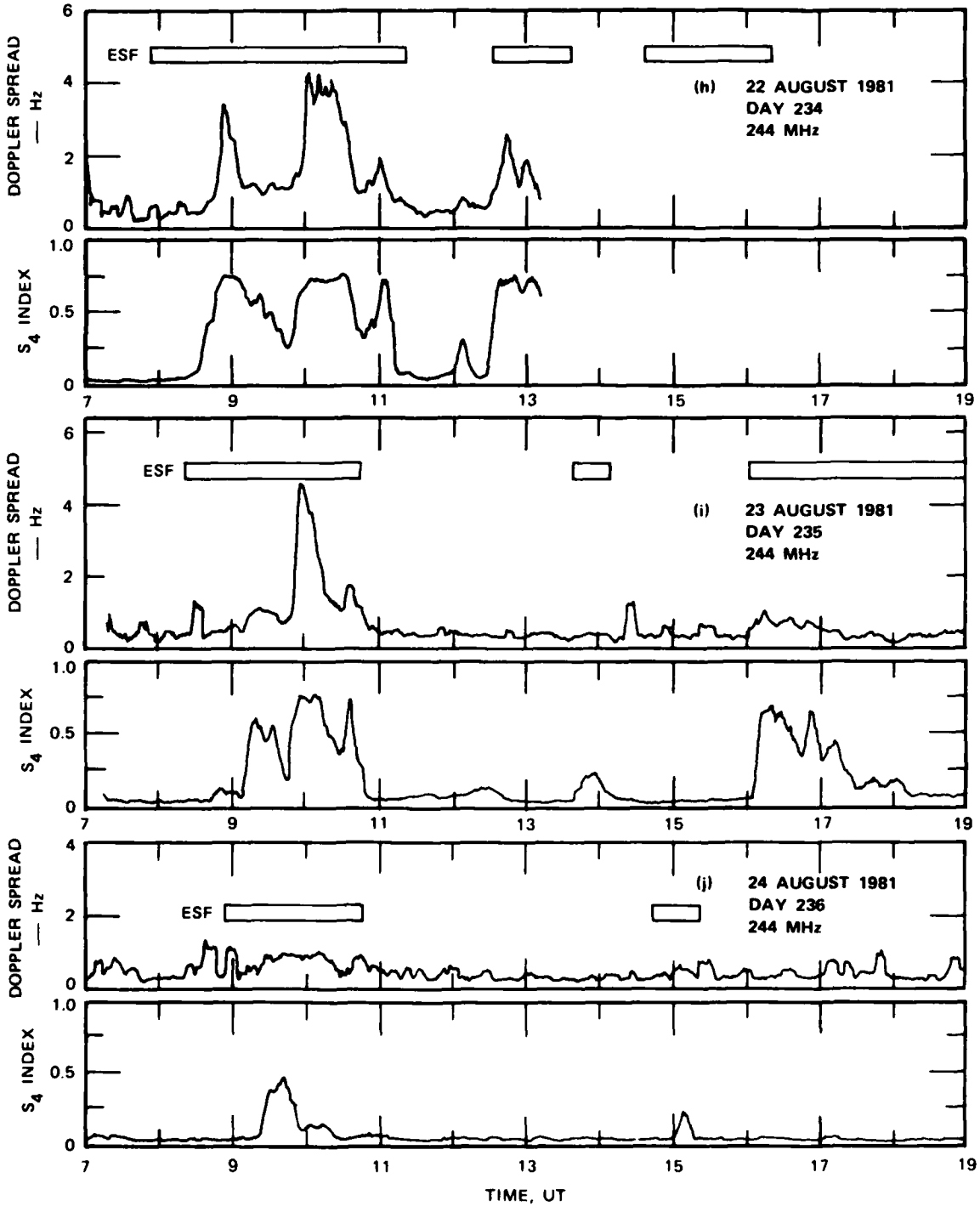

FIGURE 6 (Continued)

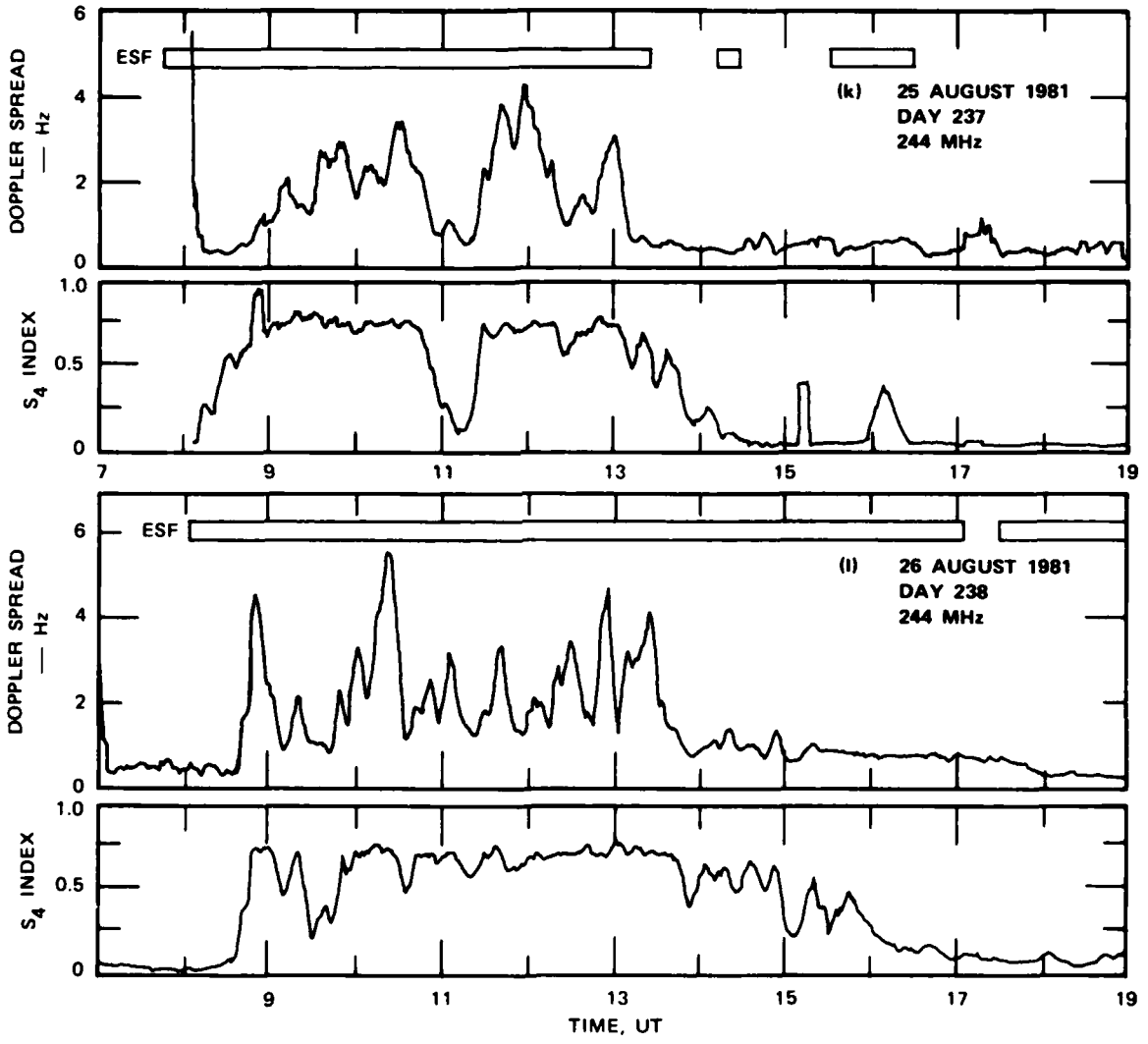

FIGURE 6 (Concluded)

Comparing the S_4 and the Doppler spread variations to ESF activity, we find good correlation. In general, ESF activity appears to commence 30 minutes to an hour before scintillation activity. The time lag between scintillation and ESF activity is most likely due to the fact that the propagation path to FLTSATCOM lies to the east of the ionosonde magnetic meridian plane. The generally eastward plasma drift carries the irregularity patches across the propagation path after they are detected in or near the meridian by the sounder. Once ESF activity begins, it appears to persist as long as the scintillations persist. We note, however, that backscatter plumes need not persist throughout the entire ESF period.[40]

We have already noted that the enhanced Doppler spread events are similar in character to backscatter plumes. The bursts of enhanced Doppler spread occur at intervals ranging from tens of minutes to a few hours. This pattern suggests an association with bottomside F-layer upwellings, and plasma bubbles. We investigate this relationship in the following subsection.

2. Doppler Spread, Upwellings, and Plasma Bubbles

In this subsection, we show the relationship between enhanced Doppler spread and F-region upwellings. Upwellings are identified by the appearance of oblique echoes on ionograms and by temporary increases in h'F (when plotted as a function of time). Recent studies have established that oblique echoes observed in ionograms during ESF conditions are produced by upwellings in the bottomside F layer.[3,4] Tsunoda[28] and Tsunoda and White[12] have shown that the upwellings are the source regions for plasma bubbles and radar backscatter plumes. Because the structuring process is believed to be most active in the vicinity of upwellings and plasma bubbles, we expect that the enhanced Doppler spread is associated with these regions.

Our preliminary comparisons are made by plotting an h'F curve together with the corresponding Doppler spread variations as shown in Figures 7 and 8. Peaks in h'F are indicated by vertical lines. In both

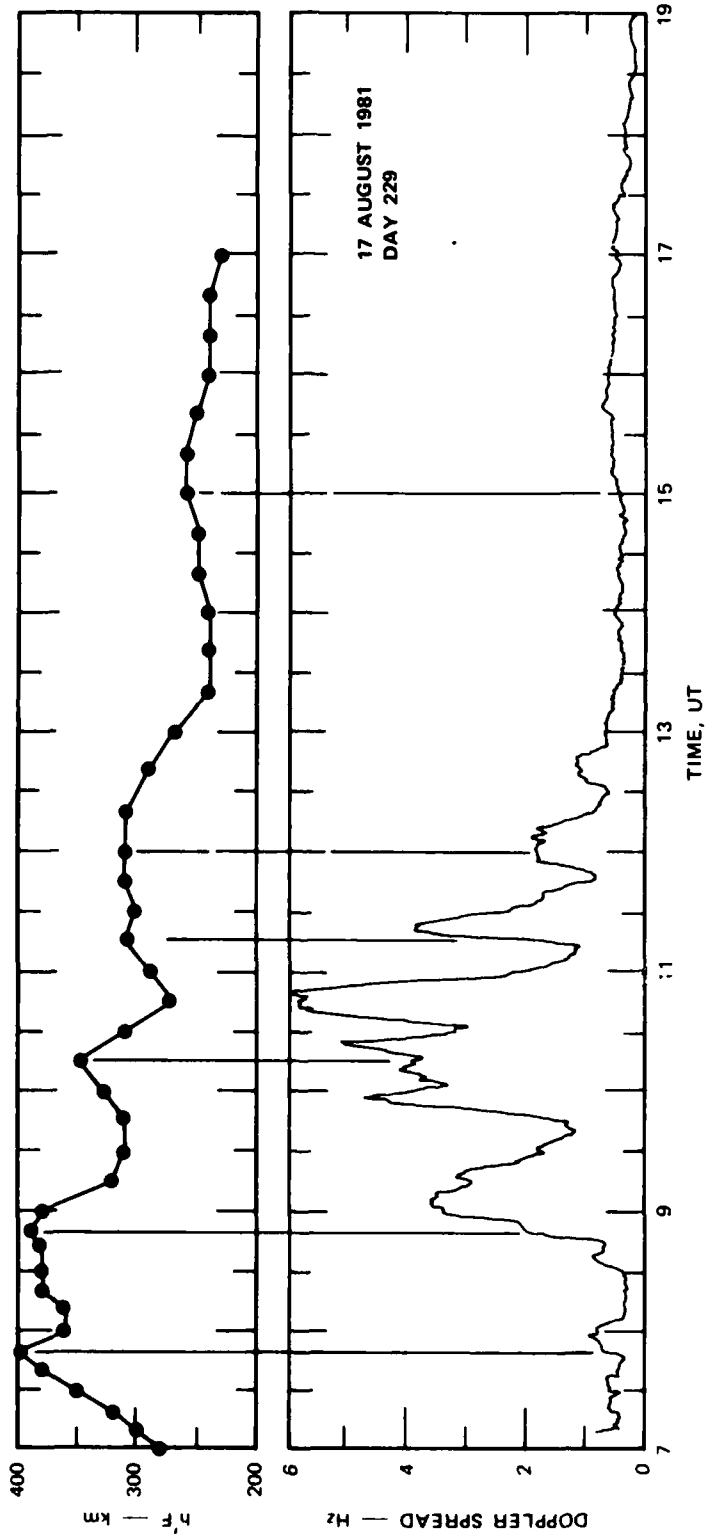

FIGURE 7 COMPARISON OF ENHANCED DOPPLER SPREAD WITH VARIATIONS IN h'F FOR DAY 229

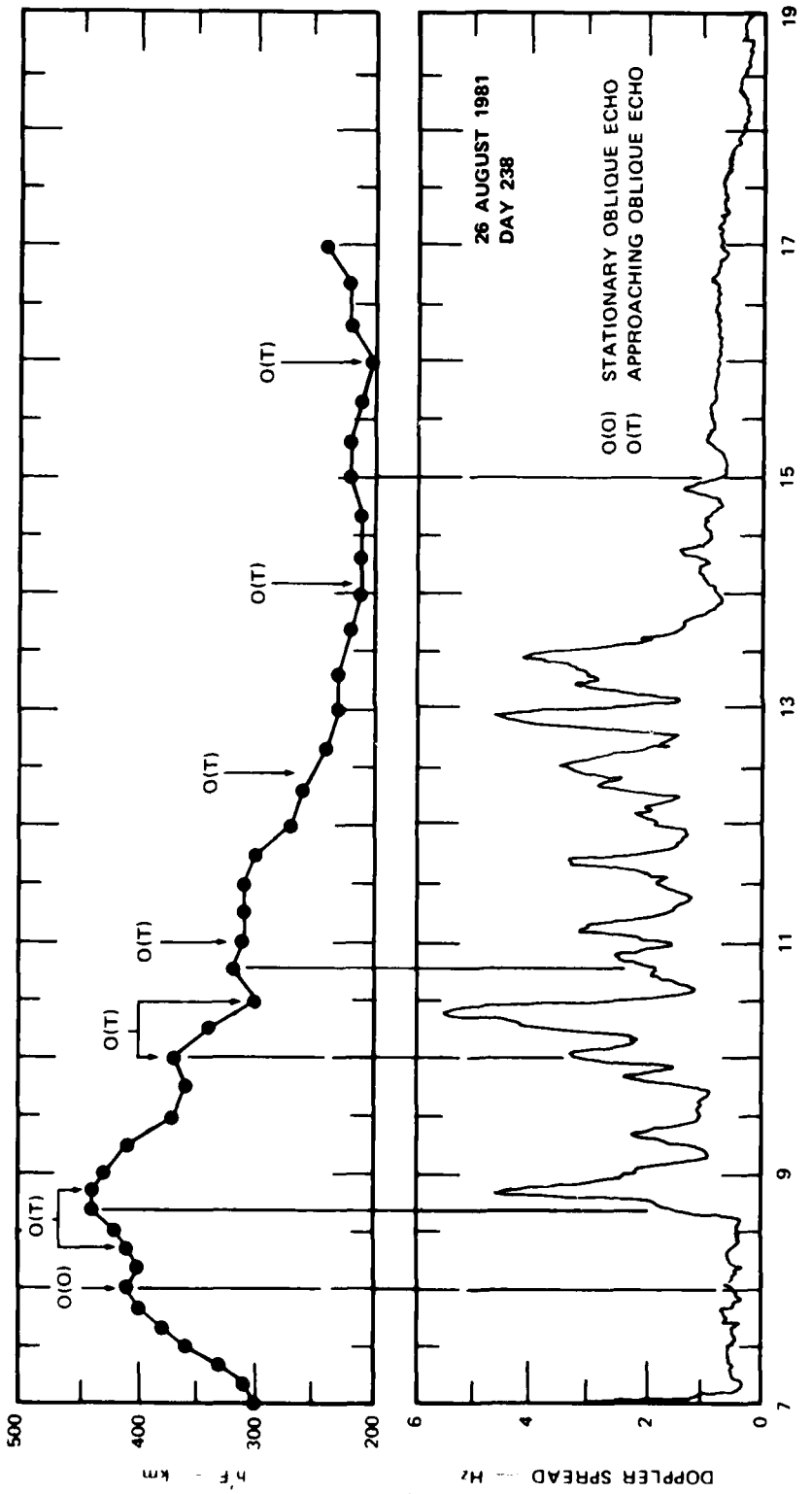

FIGURE 8 COMPARISON OF ENHANCED DOPPLER SPREAD WITH VARIATIONS IN h'F FOR DAY 238

figures the first peak (0745 in Figure 7 and 0800 in Figure 8) corresponds to the postsunset rise of the F layer and is, therefore, not associated with a true upwelling.

For the remaining events, we would expect upwellings to occur approximately ten minutes before periods of enhanced Doppler spread. In Figure 7, the Doppler spread enhancements at 0915 UT, 1040 UT, and 1115 UT admit such an association as do the enhancements at 0845 UT and 1020 UT in Figure 8. The less prominent Doppler spread peaks are evidently associated with smaller substructures within and around major upwellings that cannot be resolved by ionosonde measurements.[20] To explore this possibility in more detail we have noted the times in Figure 8 at which prominent oblique echoes were observed. All of the oblique echoes that were moving towards the main F trace are labeled with the letter T. The only stationary oblique echo (labeled 10) is seen to be associated with the postsunset rise of the F layer. All of the moving oblique echoes can be associated with enhanced Doppler spreads. We find, therefore, that periods of enhanced Doppler spread are indeed associated with upwellings in the bottomside F layer.

Encouraged by this relationship, we reanalyzed the ionograms by using a variable-speed (and reversible) movie projector to extract times at which less prominent oblique echoes appeared. These ionogram features are related to the scintillation measurements in Figure 9. We find that oblique echoes occurred throughout periods of ESF activity and that they appear to account for the maxima in Doppler spread.

These results show that local enhancements in scintillation Doppler spread are associated with the F-layer upwellings in which plumes develop and the most intense intermediate-scale irregularities have been localized. Thus, the Doppler spread measure we have developed and described is a very useful parameter for mapping the structure of intermediate-scale ESF.

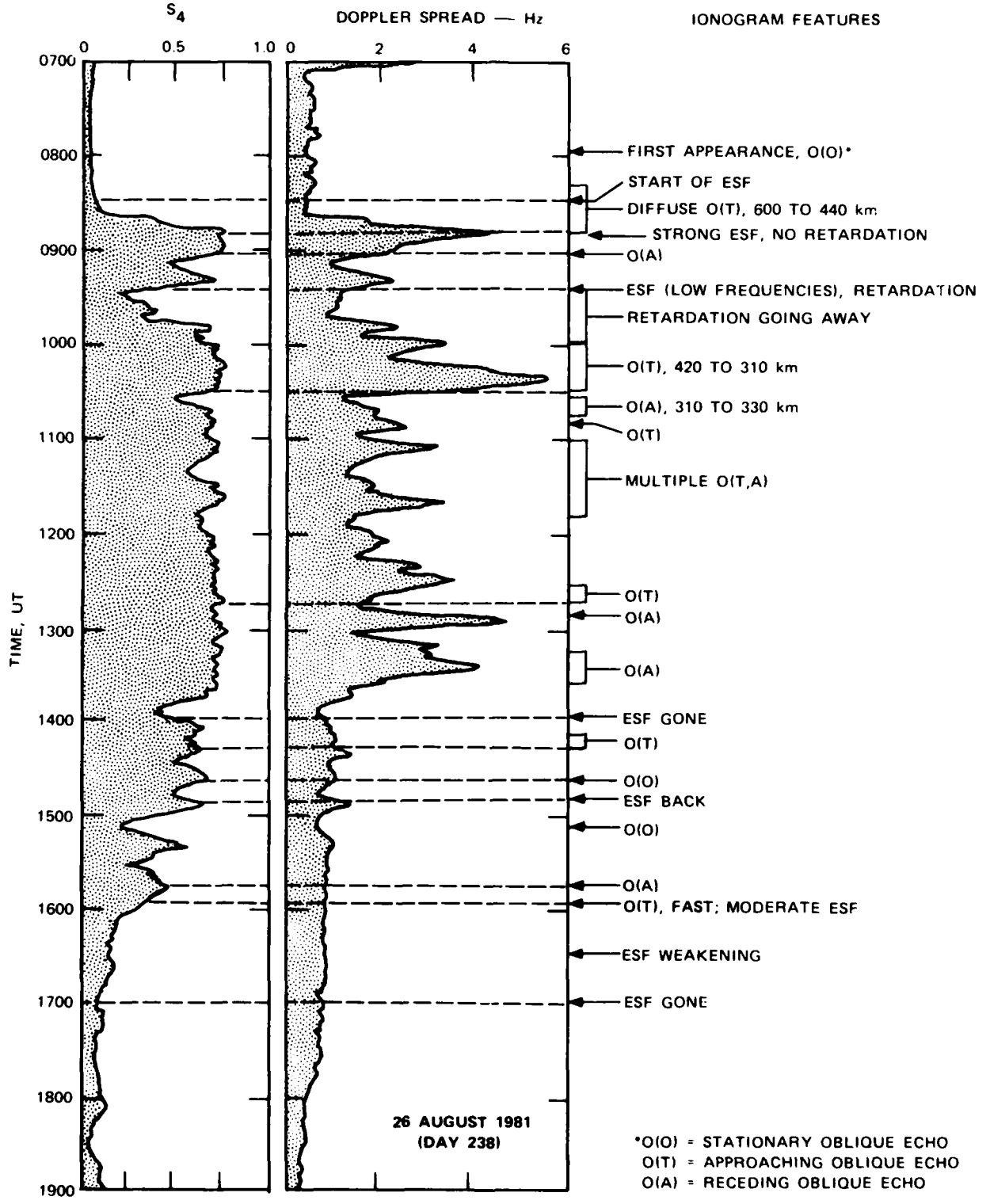

FIGURE 9 TIME CORRESPONDENCE BETWEEN VARIATIONS IN S_4 AND DOPPLER SPREAD WITH THE OCCURRENCE OF ESF AND OBLIQUE ECHOES FOR DAY 238

IV DISCUSSION AND CONCLUSIONS

In this report, we have described the results from a 1981 Kwajalein ESF experiment in which ionosonde and scintillation measurements were compared. The data that resulted from the two-week experiment are unique in that continuous measurements were made overhead of Kwajalein with high time resolution. By obtaining ionograms every 20 seconds, we were able to capture the variations in h'F and the dynamics of oblique echoes that characterize the passage of upwellings in the bottomside F layer. The continuous scintillation measurements were processed to extract the Doppler spread variations, which, we show for the first time, are the direct result of increased turbulence. From this analysis, we have established scintillation measurements as a simple monitor of upwellings and plasma bubbles.

The analysis of the ionograms included a comparison of h'F and ESF characteristics over the past five years (1977-1981). We found a definite dependence on a solar cycle that was characterized by a higher F layer and increased ESF activity during periods of higher solar activity. The behavior of the F layer over Kwajalein was consistent with those at other longitudes, in particular, that over Jicamarca, Peru. The seasonal dependence is consistent with those reported by other researchers.[46-49] The cause of the seasonal/longitudinal variation, however, remains to be explained.

The results are, however, consistent with the onset, dynamic evolution and decay of radar backscatter plumes,[28] which delineate large-scale depletions.[1] The association of enhanced Doppler spread with the upwellings or (by extrapolation) depletions is consistent with the simultaneous in situ and multifrequency scintillation measurements reported by Rino et al.[19] They found that the most intense scintillations developed in high-density regions adjacent to the depletions, hence the close association between plumes or upwellings and enhanced Doppler spread.

For the purpose of detecting regions of highly structured ionization associated with ESF, a simple VHF or UHF amplitude scintillation receiver and digital data acquisition system is very effective. The enhanced Doppler spread locates the most intense plasma microstructure. By continuously monitoring an ionosonde, the dynamics and macrostructure of the background ionosphere can be monitored. Thus, the two instruments working together provide a means of obtaining comparatively inexpensive synoptic measurements of ESF.

REFERENCES

1. J. P. McClure, W. B. Hanson, and J. H. Hoffman, "Plasma bubbles and irregularities in the equatorial ionosphere," J. Geophys. Res., 82, 2650, 1977.

2. R. F. Woodman and C. LaHoz, "Radar observations of F region equatorial irregularities," J. Geophys. Res., 81, 5447, 1976.

3. E. J. Weber, J. Buchau, R. H. Eather, and S. B. Mende, "North-south aligned equatorial airglow depletions," J. Geophys. Res., 83, 712, 1978.

4. E. J. Weber, J. Buchau, and J. G. Moore, "Airborne studies of equatorial F layer ionsopheric irregularities," J. Geophys. Res., 85, 4631, 1980.

5. S. T. Zalesak, S. L. Ossakow, and P. K. Chaturvedi, "Nonlinear equatorial spread F: The effect of neutral winds and background Pedersen conductivity," J. Geophys. Res., 87, 151, 1982.

6. S. T. Zalesak and S. L. Ossakow, "Nonlinear equatorial spread F: Spatially large bubbles resulting from large horizontal scale initial perturbations," J. Geophys. Res., 85, 2131, 1980.

7. S. L. Ossakow, S. T. Zalesak, and B. E. McDonald, "Nonlinear equatorial spread F: Dependence on altitude of the F peak and bottomside background electron density gradient scale length," J. Geophys. Res., 84, 17, 1979.

8. E. Kudeki, B. G. Fejer, D. T. Farley, and H. M. Ierkic, "Interferometer studies of equatorial F region irregularities and drifts," Geophys. Res. Lett., 8, 377, 1981.

9. R. T. Tsunoda, R. C. Livingston, and C. L. Rino, "Evidence of a velocity shear in bulk plasma motion associated with the post-sunset rise of the equatorial F layer," Geophys. Res. Lett., 8, 807, 1981.

10. R. T. Tsunoda, M. J. Baron, J. Owen, and D. M. Towle, "Altair: An incoherent scatter radar for equatorial spread F studies," Radio Sci., 14, 1111, 1979.

11. R. T. Tsunoda, "Backscatter measurements of 11-cm equatorial spread-F irregularities," Geophys. Res. Lett., 7, 848, 1980.

12. R. T. Tsunoda and B. R. White, "On the generation and growth of equatorial backscatter plumes, 1. Wave structure in the bottomside F layer," J. Geophys. Res., 86, 3610, 1981.

13. J. D. Huba, P. K. Chaturvedi, S. L. Ossakow, and D. M. Towle, "High frequency drift waves with wavelengths below the ion gyroradius in equatorial spread F," Geophys. Res. Lett., 5, 695, 1978.

14. J. D. Huba and S. L. Ossakow, "On the generation of 3-m irregularities during equatorial spread F by low-frequency drift waves," J. Geophys. Res., 84, 6697, 1979.

15. J. D. Huba and S. L. Ossakow, "On 11-cm irregularities during equatorial spread F," J. Geophys. Res., 86, 829, 1981.

16. J. L. Sperling and S. R. Goldman, "Electron collisional effects on lower hybrid drift instabilities in the ionosphere," J. Geophys. Res., 85, 3494, 1980.

17. E. P. Szuszczewicz, R. T. Tsunoda, R. Narcisi, and J. C. Holmes, "Plumex II: A second set of coincident radar and rocket observations of equatorial spread F," Geophys. Res. Lett., 8, 803, 1981.

18. E. P. Szuszczewicz, R. T. Tsunoda, R. Narcisi, and J. C. Holmes, "Coincident radar and rocket observations of equatorial spread F," Geophys. Res. Lett., 7, 537, 1980.

19. C. L. Rino, R. T. Tsunoda, J. Petriceks, R. C. Livingston, M. C. Kelley, and K. D. Baker, "Simultaneous rocket-borne beacon and in-situ measurements of equatorial spread F--intermediate wavelength results," J. Geophys. Res., 86, 2411, 1981.

20. M. C. Kelley, M. F. Larsen, C. LaHoz, and J. P. McClure, "Gravity wave initiation of equatorial spread F: A case study," J. Geophys. Res., 86, 9087, 1981.

21. R. C. Livingston, C. L. Rino, J. P. McClure, and W. B. Hanson, "Spectral characteristics of medium-scale equatorial F-region irregularities," J. Geophys. Res., 86, 2421, 1981.

22. J. Aarons, J. P. Mullen, H. E. Whitney, and E. M. MacKenzie, "The dynamics of equatorial irregularity patch formation, motion and decay," J. Geophys. Res., 45, 139, 1980.

23. B. G. Fejer, "The equatorial ionospheric electric fields. A review," J. Atmos. Terr. Phys., 43, 377, 1981.

24. R. C. Livingston, "Comparison of multifrequency equatorial scintillation: American and Pacific sectors," Radio Sci., 15, 801, 1980.

25. C. L. Rino and R. C. Livingston, "On the analysis and interpretation of spaced receiver measurements of transionospheric radio waves," Radio Sci., submitted for publication, 1982.

26. J. Aarons, J. Buchau, S. Basu, and J. P. McClure, "The localized origin of equatorial F region irregularity patches," J. Geophys. Res., 83, 1659, 1978.

27. J. A. Bittencourt and M.-A. Abdu, "A theoretical comparison between apparent and real vertical ionization drift velocities in the equatorial F region," J. Geophys. Res., 86, 2451, 1981.

28. R. T. Tsunoda, "Time evolution and dynamics of equatorial backscatter plumes, 1. Growth phase," J. Geophys. Res., 86, 139, 1981.

29. D. T. Farley, B. B. Balsley, R. F. Woodman, and J. P. McClure, "Equatorial spread F: Implications of VHF radar observations," J. Geophys. Res., 75, 7199, 1970.

30. K. Bibl, B. W. Reinisch, and S. Smith, "Equatorial spread F observations during August 1977 at Kwajalein, M. I.," preprint, University of Lowell, Lowell, MA, December 1977.

31 D. N. Anderson, "A theoretical study of the ionospheric F region equatorial anomaly--II. Results in the American and Asian sectors," Planet. Space Sci., 21, 421, 1973.

32. S. Basu, S. Basu, and B. K. Khan, "Model of equatorial scintillations from in situ measurements," Radio Sci., 11, 821, 1976.

33. W. J. Burke, D. E. Donatelli, and R. C. Sagalyn, "The longitudinal distribution of equatorial spread F plasma bubbles in the topside ionosphere," J. Geophys. Res., 85, 1335, 1980.

34. J. Aarons, J. P. Mullen, J. P. Koster, R. F. daSilva, J. R. Medeiros, R. T. Medeiros, A. Bushby, J. Pantoja, J. Lanat, and M. R. Paulson, "Seasonal and geomagnetic control of equatorial scintillations in two longitudinal sectors," J. Atmos. Terr. Phys., 42, 861, 1980.

35. R. F. Woodman, "Vertical drift velocities and east-west electric fields at the magnetic equator," J. Geophys. Res., 75, 6249, 1970.

36. R. F. Woodman, R. G. Rastogi, and C. Calderson, "Solar cycle effects on the electric fields in the equatorial ionosphere," J. Geophys. Res., 82, 5257, 1977.

37. B. G. Fejer, D. T. Farley, R. F. Woodman, and C. Calderon, "Dependence of equatorial F region vertical drifts on season and solar cycle," J. Geophys. Res., 84, 5792, 1979.

38. D. P. Sipler and M. A. Biondi, "Equatorial F-region neutral winds from nightglow OI 630.0-nm Doppler shifts," Geophys. Res. Lett., 5, 373, 1978.

39. G. Haerendel, "Theory of equatorial spread F," unpublished manuscript, Max-Planck-Inst. für Phys. und Astrophys., Inst. für extraterr. Phys., Garching, Federal Republic of Germany, 1973.

40. S. Basu and M. C. Kelley, "Review of equatorial scintillation phenomena in light of recent developments in the theory and measurement of equatorial irregularities," J. Atmos. Terr. Phys., 39, 1229, 1977.

41. C. L. Rino and J. Owen, "The time structure of transionospheric radiowave scintillation," Radio Sci., 15(3), 479, 1980.

42. C. L. Rino and J. Owen, "On the temporal coherence loss of strongly scintillating signals, Radio Sci., 16(1), 31, 1981.

43. C. L. Rino and C. H. Liu, "Intensity scintillation parameters for characterizing transionospheric radio signal," Radio Sci., accepted for publication, 1982.

44. C. L. Rino, "On the application of phase screen models to the interpretation of ionospheric scintillation data," Radio Sci., submitted for publication, 1982.

45. C. L. Rino, "Numerical computations for a one-dimensional power-law phase screen," Radio Sci., 15, 41, 1980.

46. A. J. Lyon, N. J. Skinner, and R. W. H. Wright, "The belt of equatorial spread F," J. Atmos. Terr. Phys., 19, 145, 1960.

47. B. C. Narasinga Rao, "Control of equatorial spread-F by the F-layer height," J. Atmos. Terr. Phys., 28, 1207, 1966.

48. N. J. Skinner and R. F. Kelleher, "Study of F region irregularities at Nairobi, 1.--From spread F on ionograms 1964-1970," Ann. Geophys., 27, 181, 1971.

49. H. Chandra and R. G. Rastogi, "Equatorial spread-F over a solar cycle," Ann. Geophys., 28, 709, 1972.

DISTRIBUTION LIST

DEPARTMENT OF DEFENSE

Assistant to the Secretary of Defense
Atomic Energy
ATTN: Executive Asst

Command & Control Tech Ctr
ATTN: C-650, C. Jones
ATTN: C-650
ATTN: C-312, R. Mason
3 cy ATTN: C-650, W. Heidig

Defense Communications Agency
ATTN: Code 230
ATTN: Code 205
ATTN: J300 for Yen-Sun Fu

Defense Communications Engineer Center
ATTN: Code R410
ATTN: Code R410, R. Craighill
ATTN: Code R123
ATTN Code R410, N. Jones

Defense Intelligence Agency
ATTN: DB-4C, E. O'Farrell
ATTN: DC-7B
ATTN: DB, A. Wise
ATTN: DT-1B
ATTN: DIR

Defense Nuclear Agency
ATTN: STNA
ATTN: NAFD
ATTN: RAEE
ATTN: NATD
ATTN: RAAE, P. Lunn
3 cy ATTN: RAEE
4 cy ATTN: TITL

Defense Tech Info Ctr
12 cy ATTN: DD

Dep Under Secretary of Defense
Comm, Cmd, Cont & Intell
ATTN: Dir of Intell Sys

Field Command
DNA Det 1
Lawrence Livermore Lab
ATTN: FC-1

Field Command
Defense Nuclear Agency
ATTN: FCTXE
ATTN: FCTT, G. Ganong
ATTN: FCTT, W. Summa
ATTN: FCPR

Interservice Nuc Weapons School
ATTN: TTV

Joint Chiefs of Staff
ATTN: C3S
ATTN: C3S Evaluation Office, HDOO

Joint Strat Tgt Planning Staff
ATTN: JLA, Threat Applications Div
ATTN: JLTW-2

DEPARTMENT OF DEFENSE (Continued)

National Security Agency
ATTN: R-52, J. Skillman
ATTN: B-3, F. Leonard
ATTN: W-32, O. Bartlett

Under Secy of Def for Rsch & Engrg
ATTN: Strat & Space Sys, OS
ATTN: Strat & Thtr Nuc Forces, B. Stephan

WWMCCS System Engineering Org
ATTN: J. Hoff

DEPARTMENT OF THE ARMY

Assistant Ch of Staff for Automation & Comm
ATTN: DAMO-C4, P. Kenny

US Army Electronics R&D Command
ATTN: DELAS-EO, F. Niles

BMD Advanced Tech Ctr
ATTN: ATC-R, W. Dickinson
ATTN: ATC-O, W. Davies
ATTN: ATC-T, M. Capps
ATTN: ATC-R, D. Russ

BMD Systems Command
ATTN: BMDSC-HLE, R. Webb
2 cy ATTN: BMDSC-HW

Dep Ch of Staff for Ops & Plans
ATTN: DAMO-RQC, C2 Div

Harry Diamond Labs
ATTN: DELHD-NW-P
ATTN: DELHD-NW-R, R. Williams

US Army Chemical School
ATTN: ATZN-CM-CS

US Army Comm-Elec Engrg Instal Agency
ATTN: CCC-EMEO-PED, G. Lane
ATTN: CCC-CED-CCO, W. Neuendorf

US Army Communications Command
ATTN: CC-OPS-W
ATTN: CC-OPS-WR, H. Wilson

US Army Foreign Science & Tech Ctr
ATTN: DRXST-SD

USA Missile Command
ATTN: DRSMI-YSO, J. Gamble

US Army Materiel Dev & Readiness Cmd
ATTN: DRCLDC, J. Bender

US Army Nuc & Chem Agency
ATTN: Library

US Army Satellite Comm Agency
ATTN: Doc Control

US Army White Sands Missile Range
ATTN: STEWS-TN-N, K. Cummings

DEPARTMENT OF THE ARMY (Continued)

US Army Communications R&D Command
ATTN: DRDCO-COM-RY, W. Kesselman

US Army TRADOC Sys Analysis Actvy
ATTN: ATAA-TDC
ATTN: ATAA-TCC, F. Payan Jr
ATTN: ATAA-PL

DEPARTMENT OF THE NAVY

Joint Cruise Missiles Project Ofc
ATTN: JCMG-707

Naval Air Systems Command
ATTN: PMA 271

Naval Electronic Systems Command
ATTN: Code 3101, T. Hughes
ATTN: PME-117-2013, G. Burnhart
ATTN: PME 106-13, T. Griffin
ATTN: Code 501A
ATTN: PME 106-4, S. Kearney
ATTN: PME 117-20
ATTN: PME 117-211, B. Kruger

Naval Intelligence Support Ctr
ATTN: NISC-50

Naval Ocean Systems Center
ATTN: Code 532
ATTN: Code 5323, J. Ferguson
ATTN: Code 5322, M. Paulson

Naval Research Lab
ATTN: Code 4720, J. Davis
ATTN: Code 4780, S. Ossakow
ATTN: Code 4700
ATTN: Code 4780
ATTN: Code 7500, B. Wald
ATTN: Code 6700
ATTN: Code 7950, J. Goodman
ATTN: Code 4187

Naval Space Surveillance System
ATTN: J. Burton

Naval Surface Weapons Ctr
ATTN: Code F31

Naval Telecomm Command
ATTN: Code 341

Ofc of the Deputy Chief of Naval Ops
ATTN: OP 941D
ATTN: NOP 654, Strat Eval & Anal Br
ATTN: OP 981N

Office of Naval Research
ATTN: Code 414, G. Joiner
ATTN: Code 412, W. Condell

Strat Sys Project Office
ATTN: NSP-2722, F. Wimberly
ATTN: NSP-43
ATTN: NSP-2141

Theater Nuc Warfare Prj Office
ATTN: PM-23, D. Smith

DEPARTMENT OF THE AIR FORCE

Air Force Geophysics Lab
ATTN: OPR, H. Gardiner
ATTN: OPR-1
ATTN: LKB, K. Champion
ATTN: CA, A. Stair
ATTN: PHY, J. Buchau
ATTN: R. Babcock
ATTN: R. O'Neil

Air Force Tech Applications Ctr
ATTN: TN

Air Force Weapons Lab
ATTN: SUL
ATTN: NTYC
ATTN: NTN

Air Force Wright Aeronautical Lab
ATTN: A. Johnson
ATTN: W. Hunt

Air Logistics Command
ATTN: OO-ALC/MM

Air University Library
ATTN: AUL-LSE

Assistant Ch of Staff
Studies & Analyses
ATTN: AF/SASC, C. Rightmeyer
ATTN: AF/SASC, W. Kraus

Ballistic Missile Office
ATTN: ENSN, W. Wilson
ATTN: SYC, Col Kwan

Deputy Ch of Staff
Research, Development, & Acq
ATTN: AFRDS, Space Sys & C3 Dir
ATTN: AFRDSS
ATTN: AFRDSP

Deputy Chief of Staff, Plans & Ops
ATTN: AFXOKT
ATTN: AFXOKCD
ATTN: AFXOKS

Electronic Systems Div
ATTN: ESD/SCTE, J. Clark

Electronic Systems Div
ATTN: OCT-4, J. Deas

Electronic Systems Div
ATTN: SCS-1E
ATTN: SCS-2, Lt Col, Vinkels

Foreign Tech Division
ATTN: NIIS Library
ATTN: TQTD, B. Ballard

Rome Air Development Ctr
ATTN: TSLD
ATTN: OCS, V. Coyne

Rome Air Development Ctr
ATTN: EEP, J. Rasmussen

DEPARTMENT OF THE AIR FORCE (Continued)

Space Command
ATTN: DC, T. Long

Space Division
ATTN: YGJB, W. Mercer
ATTN: YKM, Maj Alexander
ATTN: YKM, Cpt Norton

Strat Air Command
ATTN: NRT
ATTN: DCX
ATTN: XPFS
ATTN: Adwate, B. Bauer
ATTN: DCXT, T. Jorgensen

DEPARTMENT OF ENERGY

Department of Energy
ATTN: DP-233

OTHER GOVERNMENT AGENCIES

Central Intelligence Agency
ATTN: OSWR/SSD for K. Feuerpfetl
ATTN: OSWR/NED

Department of Commerce
National Bureau of Standards
ATTN: Sec Ofc for R Moore

Department of Commerce
National Oceanic & Atmospheric Admin
ATTN: R. Grubb

Institute for Telecommunications Sciences
ATTN: W. Utlaut
ATTN: A. Jean
ATTN: L. Berry

NATO

NATO School, SHAPE
ATTN: US Documents Officer

DEPARTMENT OF ENERGY CONTRACTORS

EG&G, Inc
ATTN: D. Wright
ATTN: J. Colvin

University of Calfornia
Lawrence Livermore National Lab
ATTN: Tech Info Dept Library
ATTN: L-389, R. Ott
ATTN: L-31, R. Hager

Los Alamos National Lab
ATTN: MS 664, J. Zinn
ATTN: P. Keaton
ATTN: D. Simons
ATTN: MS 670, J. Hopkins
ATTN: T. Knukle, ESS-5
ATTN: R. Jeffries
ATTN: J. Wolcott
ATTN: C. Westervelt

Sandia National Labs, Livermore
ATTN: T. Cook
ATTN: B. Murphey

DEPARTMENT OF ENERGY CONTRACTORS (Continued)

Sandia National Lab
ATTN: Space Project Div
ATTN: D. Dahlgren
ATTN: D. Thronbrough
ATTN: Tech Lib 3141
ATTN: ORG 4231, T. Wright
ATTN: ORG 1250, W. Brown

DEPARTMENT OF DEFENSE CONTRACTORS

Aerospace Corp
ATTN: V. Josephson
ATTN: T. Salmi
ATTN: I. Garfunkel
ATTN: J. Straus
ATTN: D. Olsen
ATTN: R. Slaughter

Analytical Systems Engineering Corp
ATTN: Radio Sciences

Analytical Systems Engineering Corp
ATTN: Security

BDM Corp
ATTN: L. Jacobs
ATTN: T. Neighbors

Berkeley Research Associates, Inc
ATTN: C. Prettie
ATTN: J. Workman
ATTN: S. Brecht

Boeing Aerospace Co
ATTN: MS/87-63, D. Clauson

Boeing Co
ATTN: G. Hall
ATTN: S. Tashird

BR Communications
ATTN: J. McLaughlin

University of California, San Diego
ATTN: H. Booker

Charles Stark Draper Lab, Inc
ATTN: A. Tetewski
ATTN: D. Cox
ATTN: J. Gilmore

Computer Sciences Corp
ATTN: F. Eisenbarth

COMSAT Labs
ATTN: D. Fang
ATTN: G. Hyde

Cornell University
ATTN: D. Farley Jr
ATTN: M. Kelly

E-Systems, Inc
ATTN: R. Berezdivin

Electrospace Systems, Inc
ATTN: P. Phillips
ATTN: H. Logston

DEPARTMENT OF DEFENSE CONTRACTORS (Continued)

EOS Technologies, Inc
ATTN: B. Gabbard

ESL, Inc
ATTN: J. Lehman
ATTN: R. Hechman
ATTN: R. Ibaraki
ATTN: E. Tsui
ATTN: J. Marshall

General Electric Co
ATTN: C. Zierdt
ATTN: A. Steinmayer

General Electric Co
ATTN: G. Millman

General Research Corp
ATTN: B. Bennett

Geo-Centers, Inc
ATTN: E. Marram

Harris Corp
ATTN: E. Knick

Honeywell, Inc
ATTN: G. Collyer
ATTN: G. Terry

Horizons Technology, Inc
ATTN: R. Kruger

HSS, Inc
ATTN: D. Hansen

IBM Corp
ATTN: H. Ulander

Institute for Defense Analyses
ATTN: E. Bauer
ATTN: H. Wolfhard
ATTN: J. Aein
ATTN: H. Gates

International Tel & Telegraph Corp
ATTN: Technical Library

International Tel & Telegraph Corp
ATTN: G. Wetmore

JAYCOR
ATTN: J. Sperling

Johns Hopkins University
ATTN: J. Newland
ATTN: T. Evans
ATTN: P. Komiske
ATTN: J. Phillips

Kaman Sciences Corp
ATTN: T. Stephens

Kaman Tempo
ATTN: J. Devore
ATTN: B. Gambill
ATTN: DASIAC
ATTN: K. Schwartz
ATTN: W. McNamara
ATTN: W. Knapp

DEPARTMENT OF DEFENSE CONTRACTORS (Continued)

Litton Systems, Inc
ATTN: B. Zimmer

Lockheed Missiles & Space Co, Inc
ATTN: R. Sears
ATTN: J. Kumer

Lockheed Misssiles & Space Co, Inc
ATTN: C. Old
ATTN: D. Churchill
ATTN: Dept 60-12

MIT Lincoln Lab
ATTN: D. Towle

MA/COM Linkabit Inc
ATTN: I. Jacobs
ATTN: A. Viterbi
ATTN: H. Van Trees

Magnavox Govt & Indus Electronics Co
ATTN: G. White

Martin Marietta Corp
ATTN: R. Heffner

McDonnel Douglas Corp
ATTN: R. Halprin
ATTN: H. Spitzer
ATTN: Tech Library Svcs
ATTN: W. Olson

Meteor Communications Corp
ATTN: R. Leader

Mission Research Corp
ATTN: R. Bigoni
ATTN: Tech Library
ATTN: R. Kilb
ATTN: G. McCartor
ATTN: F. Guigliano
ATTN: R. Bogusch
ATTN: S. Gutsche
ATTN: F. Fajen
ATTN: R. Hendrick
ATTN: C. Lauer

Mitre Corp
ATTN: A. Kymmel
ATTN: MS J104/M, R. Dresp
ATTN: G. Harding
ATTN: C. Callahan

Mitre Corp
ATTN: W. Foster
ATTN: M. Horrocks
ATTN: J. Wheeler
ATTN: W. Hall

Pacific-Sierra Research Corp
ATTN: E. Field Jr
ATTN: H. Brode, Chairman SAGE
ATTN: F. Thomas

Pennsylvania State University
ATTN: Ionospheric Research Lab

Photometrics, Inc
ATTN: I. Kofsky

DEPARTMENT OF DEFENSE CONTRACTORS (Continued)

Physical Dynamics, Inc
ATTN: E. Fremouw

Physical Research, Inc
ATTN: R. Deliberis

R&D Associates
ATTN: W. Wright
ATTN: R. Turco
ATTN: R. Lelevier
ATTN: W. Karzas
ATTN: C. Greifinger
ATTN: F. Gilmore
ATTN: H. Ory
ATTN: M. Gantsweg

R&D Associates
ATTN: B. Yoon

Rand Corp
ATTN: C. Crain
ATTN: E. Bedrozian

Riverside Research Institute
ATTN: V. Trapani

Rockwell International Corp
ATTN: R. Buckner

Rockwell International Corp
ATTN: S. Quilici

Santa Fe Corp
ATTN: D. Paolucci

Science Applications, Inc
ATTN: C. Smith
ATTN: E. Straker
ATTN: D. Hamlin
ATTN: L. Linson

Science Applications, Inc
ATTN: J. Cockayne

Stewart Radiance Lab
ATTN: J. Ulwich

DEPARTMENT OF DEFENSE CONTRACTORS (Continued)

Sylvania Systems Group
ATTN: R. Steinhoff

Utah State University
ATTN: D. Burt
ATTN: K. Baker, Dir Atmos & Space Science
ATTN: L. Jensen, Elec Eng Dept
ATTN: A. Steed

Sylvania Systems Group
ATTN: I. Kohlberg
ATTN: J. Concordia

Technology International Corp
ATTN: W. Boquist

TRI-COM, Inc
ATTN: D. Murray

TRW Electronics & Defense Sector
ATTN: G. Kirchner
ATTN: R. Plebuch

VisiDyne, Inc
ATTN: C. Humphrey
ATTN: W. Reidy
ATTN: J. Carpenter
ATTN: O. Shepard

SRI International
ATTN: G. Price
ATTN: W. Chesnut
ATTN: M. Baron
ATTN: D. McDaniels
ATTN: D. Neilson
ATTN: R. Livingston
ATTN: R. Leadabrand
ATTN: A. Burns
ATTN: J. Petrickes
ATTN: G. Smith
ATTN: W. Jaye
ATTN: V. Gonzales
ATTN: J. Vickrey
4 cy ATTN: C. Rino
4 cy ATTN: R. Tsunoda